

Effect of nuclear vibration on high-order-harmonic generation of aligned H_2^+ moleculesDmitry A. Telnov,^{1,*} John Heslar,^{2,†} and Shih-I Chu^{2,3,‡}¹*Department of Physics, St. Petersburg State University, St. Petersburg 198504, Russia*²*Department of Physics, Center for Quantum Science and Engineering and Center for Advanced Study in Theoretical Sciences, National Taiwan University, Taipei 10617, Taiwan*³*Department of Chemistry, University of Kansas, Lawrence, Kansas 66045, USA*

(Received 23 September 2014; published 4 December 2014)

High-order-harmonic generation (HHG) spectra have been calculated for H_2^+ molecules aligned parallel to the polarization of the laser field. We make use of the Jacobi coordinates and neglect the rotation of the nuclei. The remaining time-dependent Schrödinger equation is three dimensional in spatial coordinates, one of them being the internuclear separation and the other two describing the electronic motion. The problem is solved using the accurate and efficient time-dependent generalized pseudospectral method in prolate spheroidal coordinates for the electronic coordinates and Fourier grid method for the internuclear separation. Laser pulses with a carrier wavelength of 800 nm, a duration of ten optical cycles, and a peak intensity of 2×10^{14} W/cm² have been used in the calculations. Our HHG spectra, which incorporate the effect of nuclear vibration, generally exhibit a significant deviation from those calculated for the fixed internuclear separations. The low-energy regions of the spectra, however, resemble those for the nuclei fixed at larger separations, while the high-energy regions are closer to those for the nuclei fixed at smaller internuclear distances. The dynamics of the nuclear vibrational wave packet is also obtained and analyzed.

DOI: [10.1103/PhysRevA.90.063412](https://doi.org/10.1103/PhysRevA.90.063412)

PACS number(s): 33.80.Rv, 42.65.Ky

I. INTRODUCTION

High-order-harmonic generation (HHG) is a fundamental atomic and molecular process in strong laser fields that remains a subject of much current interest in science and technology [1]. Novel phenomena including generation of attosecond pulses [2,3] and ultrafast molecular imaging [4,5] are also closely related to HHG. With laser pulses as short as a few femtoseconds, HHG spectroscopy can become a possible tool for probing chemical reactions on a femtosecond time scale.

Small diatomic molecules subject to intense laser fields continue attracting much attention and have been a subject of many experimental and theoretical investigations (see the reviews [6,7], and references therein). Due to the extra degrees of freedom, even the simplest molecules show considerably more complicated responses to strong fields than that of atoms and pose additional challenge to researchers. Substantial efforts have been made to study the dependence of the HHG signal on the orientation of the molecular axis with respect to the polarization of the laser field and related two-center interference phenomena [8–10].

Many theoretical studies of HHG in molecules use the fixed-nuclei approximation and treat only the electron motion (see, for example, [9,11,12]; more references can be found in the review paper [7]). This is a reasonable approximation since the nuclear motion is generally much slower than the electron motion. On the other hand, the period of nuclear vibration can be as short as 10–20 fs, which is comparable with the duration of driving laser pulses. Thus the influence of the nuclear vibration on production of high harmonics may be significant. There are several studies that include nuclear motion in the HHG theory and calculations [13–19].

An accurate *ab initio* treatment of all electronic and nuclear degrees of freedom is still beyond the capabilities of modern computational equipment even for the simplest one-electron molecule H_2^+ . Thus most of the existing results are based on simplified models, which involve the Born-Oppenheimer approximation [14,15,18,19] (for consistent formulation of the time-dependent Born-Oppenheimer approximation, see Refs. [20,21]) or reduced dimensionality [13,16,17]. The theories of Refs. [18,19] treat the harmonic yield as a sum of contributions corresponding to different internuclear separations and weighted by the nuclear wave-packet distribution. It was observed that the harmonic signal is very sensitive to the bond length [18], so an accurate description of the nuclear dynamics including nonadiabatic effects and the influence of the driving laser field may be very important.

The motivation of this paper is to provide accurate benchmark results regarding the high-order-harmonic yield and nuclear vibrational dynamics of the hydrogen molecular ions H_2^+ subject to short intense laser pulses. Here we report three-dimensional calculations of HHG in H_2^+ aligned parallel to the polarization of the laser field. Our approach treats the electron motion in full dimensionality and includes nonadiabatically the effect of nuclear vibration. Only the nuclear rotation is neglected, but its effect may not be very important for aligned molecules and short laser pulses. The paper is organized as follows. In Sec. II we discuss our theoretical and computational approach, introducing the Jacobi coordinates for H_2^+ and describing the numerical procedure. In Sec. III we present our results regarding the dynamics of the nuclear wave packet and HHG spectra. Section IV contains a summary.

II. THEORETICAL AND COMPUTATIONAL METHOD**A. Jacobi coordinates for H_2^+**

Originally, the system is described by the radius vectors of the nuclei \mathbf{R}_1 and \mathbf{R}_2 and the electron \mathbf{r}_e in the laboratory

*telnov@pcqnt1.phys.spbu.ru

†john.heslar@gmail.com

‡sichu@ku.edu

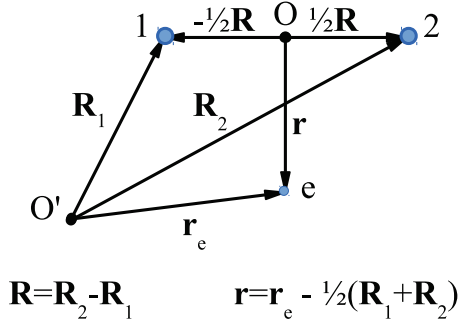


FIG. 1. (Color online) Jacobi coordinates for H_2^+ . The nuclei are denoted by 1 and 2 and the electron is denoted by e ; O is the center of mass of the nuclei and O' is the center of the laboratory frame.

frame of reference with the center O' (see Fig. 1). The Jacobi coordinates are the relative radius vector of the nuclei \mathbf{R} , the radius vector of the electron with respect to the center of mass of the nuclei \mathbf{r} , and the radius vector of the center of mass of the whole system \mathbf{R}_c (Fig. 1):

$$\mathbf{R} = \mathbf{R}_2 - \mathbf{R}_1, \quad (1)$$

$$\mathbf{r} = \mathbf{r}_e - \frac{1}{2}(\mathbf{R}_1 + \mathbf{R}_2), \quad (2)$$

$$\mathbf{R}_c = \frac{m}{2M+m}\mathbf{r}_e + \frac{M}{2M+m}(\mathbf{R}_1 + \mathbf{R}_2), \quad (3)$$

where M and m are the proton and electron masses, respectively. In the laboratory frame, the unperturbed Hamiltonian of H_2^+ reads (we use atomic units, but indicate explicitly the electron mass m)

$$H_0 = -\frac{1}{2M}\nabla_1^2 - \frac{1}{2M}\nabla_2^2 - \frac{1}{2m}\nabla_e^2 + \frac{1}{|\mathbf{R}_2 - \mathbf{R}_1|} - \frac{1}{|\mathbf{r}_e - \mathbf{R}_1|} - \frac{1}{|\mathbf{r}_e - \mathbf{R}_2|}, \quad (4)$$

where ∇_1 , ∇_2 , and ∇_e are the differential operators with respect to \mathbf{R}_1 , \mathbf{R}_2 , and \mathbf{r}_e . Upon transformation to the Jacobi coordinates, the Hamiltonian takes the form

$$H_0 = T_R + T_r + T_c + \frac{1}{R} - \frac{1}{|\mathbf{r} - \frac{1}{2}\mathbf{R}|} - \frac{1}{|\mathbf{r} + \frac{1}{2}\mathbf{R}|}. \quad (5)$$

The first term on the right-hand side of Eq. (5) represents the kinetic energy of the relative (vibrational and rotational) nuclear motion; the reduced mass of the proton is equal to $M/2$,

$$T_R = -\frac{1}{M}\nabla_R^2. \quad (6)$$

The second term is the kinetic energy of the electron

$$T_r = -\frac{1}{2\mu}\nabla_r^2. \quad (7)$$

The reduced mass of the electron μ is expressed as follows:

$$\mu = \frac{2Mm}{2M+m}. \quad (8)$$

The third term is the kinetic energy of the center of mass

$$T_c = -\frac{1}{2(2M+m)}\nabla_c^2. \quad (9)$$

In Eqs. (6), (7), and (9) the differential operators ∇_R , ∇_r , and ∇_c are defined with respect to \mathbf{R} , \mathbf{r} , and \mathbf{R}_c as independent variables.

The interaction with the laser field is described in the dipole approximation, which is well justified for the wavelengths in the near-infrared band. In the laboratory frame, the interaction term in the Hamiltonian can be written as follows: using the length gauge

$$H_I^L = \mathbf{F} \cdot (\mathbf{r}_e - \mathbf{R}_1 - \mathbf{R}_2) \quad (10)$$

or velocity gauge

$$H_I^V = -\frac{i}{c}\mathbf{A} \cdot \left(\frac{1}{m}\nabla_e - \frac{1}{M}\nabla_1 - \frac{1}{M}\nabla_2 \right), \quad (11)$$

c being the speed of light. In Eqs. (10) and (11), the vector potential \mathbf{A} and the field strength \mathbf{F} depend on the time only; they are related to each other as

$$\mathbf{F}(t) = -\frac{1}{c}\frac{d}{dt}\mathbf{A}(t). \quad (12)$$

In Eq. (11) we have omitted the terms proportional to A^2 . In the dipole approximation, they depend on the time only and do not cause transitions between different quantum states. In the Jacobi coordinates, the interaction terms (10) and (11) are transformed as follows:

$$H_I^L = \left(1 + \frac{m}{2M+m} \right) \mathbf{F} \cdot \mathbf{r} - \mathbf{F} \cdot \mathbf{R}_c, \quad (13)$$

$$H_I^V = -\frac{i(M+m)}{Mmc}\mathbf{A} \cdot \nabla_r + \frac{i}{(2M+m)c}\mathbf{A} \cdot \nabla_c. \quad (14)$$

Note that the relative nuclear motion (described by the vector \mathbf{R}) is not coupled to the external field.

B. Aligned H_2^+ molecules in the laser field

For aligned molecules, we can neglect the nuclear rotation and retain only vibration in the nuclear kinetic energy. Then the kinetic energy operator T_R reduces to its radial part

$$T_R \rightarrow -\frac{1}{M}\left[\frac{\partial^2}{\partial R^2} + \frac{2}{R}\frac{\partial}{\partial R} \right]. \quad (15)$$

Such an approximation has been widely used for aligned molecules (see, for example, [22–24], and references therein). After separation of the center-of-mass motion, the total time-dependent Hamiltonian is four dimensional and can be written as follows (the length gauge is used for the interaction with the laser field):

$$H(t) = -\frac{1}{M}\left[\frac{\partial^2}{\partial R^2} + \frac{2}{R}\frac{\partial}{\partial R} \right] + \frac{1}{R} - \frac{1}{2\mu}\nabla_r^2 - \frac{1}{|\mathbf{r} - \frac{1}{2}\mathbf{R}|} - \frac{1}{|\mathbf{r} + \frac{1}{2}\mathbf{R}|} + \left(1 + \frac{m}{2M+m} \right) \mathbf{F}(t) \cdot \mathbf{r}. \quad (16)$$

For the laser field polarized along the molecular axis, the projection of the electron angular momentum on the molecular axis is conserved and the problem is reduced to three dimensions. Using prolate spheroidal coordinates for the electron radius vector \mathbf{r} , the Hamiltonian (16) is represented as follows:

$$H(t) = H_0 + V(t), \quad (17)$$

$$H_0 = -\frac{1}{M} \left[\frac{\partial^2}{\partial R^2} + \frac{2}{R} \frac{\partial}{\partial R} \right] + \frac{1}{R} - \frac{2}{\mu R^2} \frac{1}{(\xi^2 - \eta^2)} \left[\frac{\partial}{\partial \xi} (\xi^2 - 1) \frac{\partial}{\partial \xi} + \frac{\partial}{\partial \eta} (1 - \eta^2) \frac{\partial}{\partial \eta} - \frac{m_z^2}{\xi^2 - 1} - \frac{m_z^2}{1 - \eta^2} \right] - \frac{4\xi}{R(\xi^2 - \eta^2)}, \quad (18)$$

$$V(t) = \frac{1}{2} \left(1 + \frac{m}{2M + m} \right) F(t) R \xi \eta, \quad (19)$$

where m_z is the projection of the electron angular momentum on the molecular (z) axis.

The time-dependent Schrödinger equation

$$i \frac{\partial}{\partial t} \Psi(\xi, \eta, R, t) = H(t) \Psi(\xi, \eta, R, t) \quad (20)$$

for the Hamiltonian (17) is solved using the time-dependent generalized pseudospectral method [25]. The coordinates ξ and η are discretized with the help of the generalized pseudospectral (GPS) method, applying the Gauss-Legendre set of collocation points for η and the Gauss-Radau set for ξ [10,26]. For discretization of the R coordinate, we apply the Fourier grid (FG) method [27]. For the time evolution of the wave function, we employ the following split-operator, second-order short-time propagation formula:

$$\begin{aligned} \Psi(t + \Delta t) &= \exp \left(-\frac{i}{2} \Delta t H_0 \right) \\ &\times \exp \left[-i \Delta t V \left(t + \frac{1}{2} \Delta t \right) \right] \\ &\times \exp \left(-\frac{i}{2} \Delta t H_0 \right) \Psi(t) + O((\Delta t)^3). \end{aligned} \quad (21)$$

Here Δt is the time propagation step. The operator $\exp(-\frac{i}{2} \Delta t H_0)$ is constructed by the spectral expansion

$$\exp \left(-\frac{i}{2} \Delta t H_0 \right) = \sum_n \exp \left(-\frac{i}{2} \Delta t E_n \right) |\psi_n\rangle \langle \psi_n|, \quad (22)$$

where ψ_n and E_n are the eigenvectors and eigenvalues, respectively, of the unperturbed Hamiltonian H_0 (18). In practical calculations, the summation in (22) includes all eigenvectors with the energies $E_n < E_b$, where the upper limit E_b should be large enough to describe all relevant physical processes. With the control of high-energy contributions to the propagator matrix, we can avoid the population of physically irrelevant regions of the energy spectrum and improve numerical stability of the computations. In the present work, we use $E_b = 10$ a.u. For the carrier wavelength 800 nm and peak intensity 2×10^{14} W/cm², this value of E_b is approximately equal to $23U_p$ (U_p is the ponderomotive potential), which is well in excess of the expected cutoff energy of the HHG spectrum. For the given Δt , the propagator matrix $\exp(-\frac{i}{2} \Delta t H_0)$ is time independent

and constructed only once before the propagation process starts. The matrix $\exp[-i \Delta t V(t + \frac{1}{2} \Delta t)]$ is time dependent and must be calculated at each time step. However, for the interaction with the laser field in the length gauge, this matrix is diagonal in both the GPS and FG methods and its calculation is not time consuming (all potential terms are represented by their values on the coordinate grid and appear as diagonal matrices; no calculation of potential energy matrix elements is required).

The problem is solved in the box with the linear dimension of $r_b = 43$ a.u. for the electronic motion. The box size must be large enough to accommodate electron excursions in the laser field (the excursion amplitude is about 23 a.u. for the chosen field parameters); on the other hand, it should be kept as small as possible to make the calculations more accurate with the same number of grid points. The internuclear distance R is restricted to the interval $[0.75, 8.75]$, which is large enough to contain the nuclear wave packet during the laser pulse. To achieve sufficient accuracy, we use 88 grid points in ξ , 24 grid points in η , and 31 grid points in R (the total linear dimension of the Hamiltonian matrix is 65472). In the present work, we use 4096 time steps per optical cycle; this is enough to achieve convergence for the wavelength and intensity used in the calculations. In intense laser fields, ionization can be significant. In our present calculations, the ionized parts of the electronic wave packet are collected by an absorber placed in a layer between r_b and $r_a = 23$ a.u. The absorber prevents spurious reflections from the box boundary at $r = r_b$. Because of the absorber, the normalization of the wave function decreases in time. The ionization probability can be calculated from the normalization of the wave function at the end of the laser pulse. We do not use an absorber for the nuclear motion. Our laser pulse is quite short and the nuclear wave packet does not reach the boundary at $R = 8.75$ a.u. by the end of the pulse.

III. RESULTS AND DISCUSSION

To construct the short-time propagator (22), we solve an eigenvalue problem for the Hamiltonian H_0 (18) and obtain the unperturbed energy eigenvalues and eigenfunctions of H_2^+ . Although the Hamiltonian (18) neglects rotation of the nuclei, it includes the nuclear vibration on the same footing as the electronic motion, so the eigenvalues and eigenfunctions are obtained beyond the Born-Oppenheimer approximation. The low-lying energy eigenvalues are listed in Table I. As one can

TABLE I. Low-lying vibrational eigenvalues of H_2^+ (a.u.): (a) present calculations for aligned molecules with no rotation and (b) fully nonadiabatic rovibrational eigenvalues for the total angular momentum $J = 0$ [28].

v	(a)	(b)
0	-0.59723	-0.59714
1	-0.58725	-0.58716
2	-0.57785	-0.57775
3	-0.56899	-0.56891
4	-0.56064	-0.56061
5	-0.55297	-0.55284

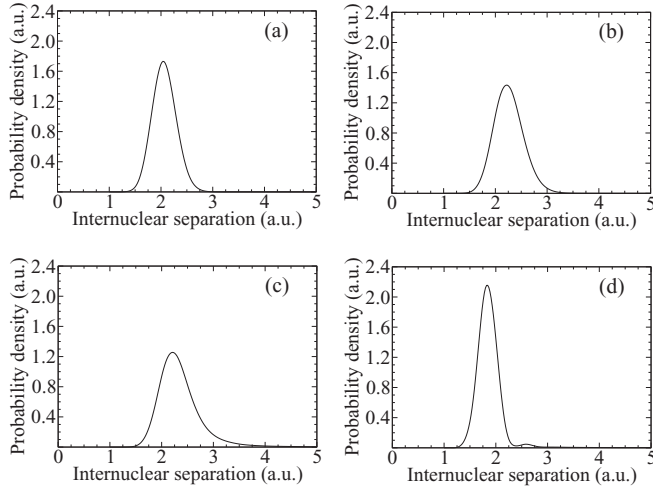


FIG. 2. Nuclear density distribution of H_2^+ initially in the ground state ($v = 0$) at different times for the peak intensity of the laser field $2 \times 10^{14} \text{ W/cm}^2$: (a) $t = 0$, (b) $t = 5$ optical cycles, (c) $t = 8$ optical cycles, and (d) $t = 10$ optical cycles.

see, our energies are slightly lower than the corresponding rovibrational eigenvalues for the total angular momentum $J = 0$ from the accurate variational calculations [28]. We can estimate the order of magnitude of the contribution to the energies due to the nuclear rotation as 10^{-4} a.u.

The laser pulse $F(t)$ has a \sin^2 envelope with the carrier wavelength 800 nm and total duration of 10 optical cycles. Here we report the results for the peak intensity $2 \times 10^{14} \text{ W/cm}^2$. With the total time-dependent electron and nuclear wave function $\Psi(\xi, \eta, R, t)$ we can calculate the spectrum of emitted harmonics and analyze the motion of the nuclear wave packet.

A. Dynamics of the nuclear wave packet

The probability density for the nuclear motion $\rho_n(R, t)$ is obtained from the total wave function after integration over the electronic coordinates

$$\rho_n(R, t) = \int d^3r |\Psi(\mathbf{r}, R, t)|^2. \quad (23)$$

The time evolution of the nuclear wave packet is shown in Figs. 2 and 3 for the molecule initially in the vibrational states $v = 0$ and 1, respectively. When the laser field is switched on, the position and shape of the nuclear wave packet change very little until the field becomes strong enough [approximately, when the time t becomes greater than four optical cycles (OCs) of the 800-nm radiation]. The peak intensity is reached at $t = 5$ OCs; at this time, transitions to the excited vibrational states become significant and evolution of the nuclear wave packet can be seen clearly. At first, the center of the nuclear wave packet moves towards larger internuclear separations and the packet itself broadens. Approximately at $t = 7$ OCs, the direction of the motion is reversed. At the end of the laser pulse ($t = 10$ OCs), the distribution is narrower than the initial nuclear wave packet at $t = 0$ and its center is shifted to smaller internuclear distance. For the ground initial state ($v = 0$), the distribution preserves its bell shape throughout the time evolution. For the first excited initial state ($v = 1$), the distribution

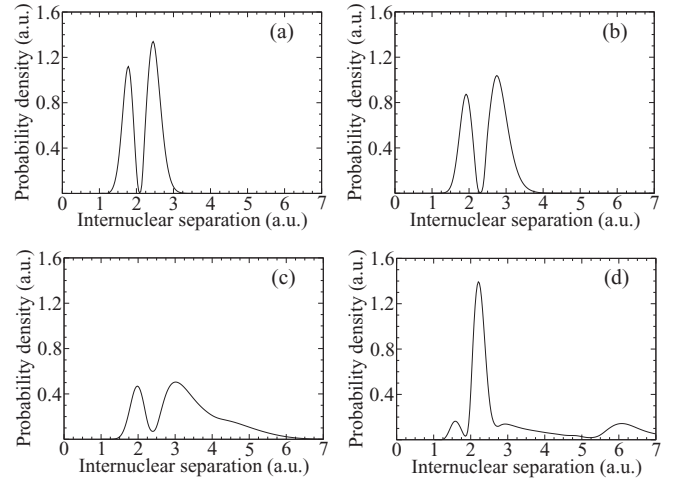


FIG. 3. Nuclear density distribution of H_2^+ initially in the first excited state ($v = 1$) at different times for the peak intensity of the laser field $2 \times 10^{14} \text{ W/cm}^2$: (a) $t = 0$, (b) $t = 5$ optical cycles, (c) $t = 8$ optical cycles, and (d) $t = 10$ optical cycles.

at $t = 0$ has two peaks, with the right peak slightly larger than the left one. At the end of the laser pulse, the right peak appears much larger than the left one. Since the whole distribution is shifted to smaller internuclear distances at $t = 10$ OCs, the suppression of the left peak can be explained by steepening of the repulsive internuclear potential towards smaller internuclear separations. Unlike the case $v = 0$ in the initial state, dissociation caused by the interaction with the laser pulse is quite significant for $v = 1$. At $t = 10$ OCs [Fig. 3(d)] one can see a substantial portion of the nuclear wave packet around $R = 6$ a.u. moving towards larger internuclear distances.

The oscillation period T_n of the nuclear wave packet can be estimated as 15 fs, according to the equation $T_n = 2\pi/\omega_n$, where the frequency ω_n is calculated as the difference between the energies of the levels with $v = 1$ and 0. This estimate is in fair agreement with our results, since 1 OC = 2.67 fs for the 800-nm radiation and one-half of the nuclear vibration period is approximately equal to 3 OCs.

B. The HHG spectra

To calculate the HHG spectra, we employ the widely used semiclassical approach, where the basic expressions come from the classical electrodynamics but the classical quantities such as dipole moment and its acceleration are replaced with the corresponding quantum expectation values. The spectral density of the radiation energy is given by the following expression [29]:

$$S(\omega) = \frac{2}{3\pi c^3} |\tilde{\mathbf{a}}(\omega)|^2, \quad (24)$$

$$\tilde{\mathbf{a}}(\omega) = \int_{-\infty}^{\infty} dt \mathbf{a}(t) \exp(i\omega t), \quad (25)$$

where c is the speed of light. The time-dependent dipole acceleration $\mathbf{a}(t)$ has an obvious relation with the dipole moment $\mathbf{d}(t)$,

$$\mathbf{a}(t) = \frac{d^2}{dt^2} \mathbf{d}(t), \quad (26)$$

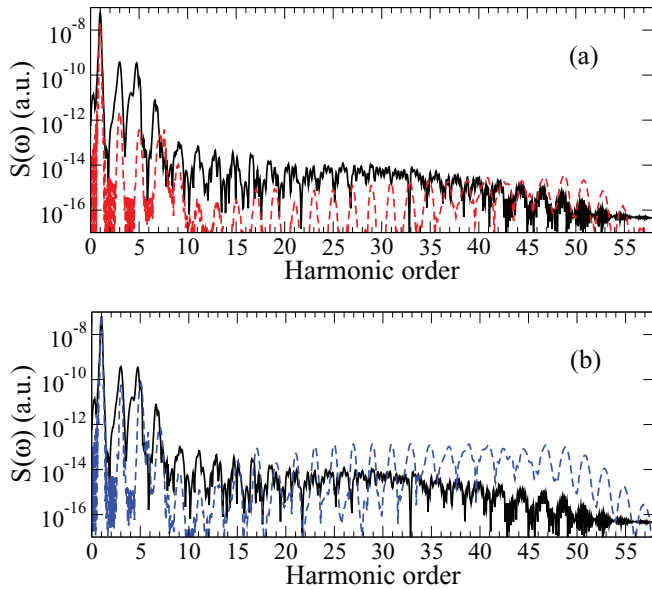


FIG. 4. (Color online) Plot of the HHG spectra for the initial vibrational level $v = 0$ and the laser peak intensity 2×10^{14} W/cm² (black solid line). Also shown are the HHG spectra for the fixed nuclei at internuclear separations of (a) 2 a.u. (red dashed line) and (b) 2.4 a.u. (blue dashed line).

and the dipole moment is calculated as a quantum expectation value

$$\mathbf{d}(t) = \langle \Psi | \mathbf{R}_1 + \mathbf{R}_2 - \mathbf{r}_e | \Psi \rangle. \quad (27)$$

The expectation value of the dipole acceleration can be derived from Eq. (27) with the help of the Ehrenfest theorem. Upon transformation to the Jacobi coordinates, one obtains

$$\begin{aligned} \mathbf{a}(t) = & -\frac{M+m}{Mm} \langle \Psi | \nabla_r \left[\frac{1}{|\mathbf{r} - \frac{1}{2}\mathbf{R}|} + \frac{1}{|\mathbf{r} + \frac{1}{2}\mathbf{R}|} \right] | \Psi \rangle \\ & + \frac{M+2m}{Mm} \mathbf{F}(t). \end{aligned} \quad (28)$$

In Fig. 4 we show the HHG spectrum $S(\omega)$ for H_2^+ initially in the ground state $v = 0$. Also shown are the spectra obtained in the fixed-nuclei approximation at the internuclear distances $R = 2$ and 2.4 a.u. According to the well-known semiclassical recollision model [30], the cutoff of the HHG spectrum is expected at the photon energy $I_p + 3.17U_p$, where I_p is the ionization potential of the target. For the laser field parameters used in the calculations and vertical ionization potentials of H_2^+ at $R = 2$ and 2.4 a.u., the cutoff energy corresponds to the harmonic orders 44 and 42, respectively. The HHG spectra for both the fixed and vibrating nuclei show well-pronounced cutoffs in fair agreement with the semiclassical prediction. As one can see, the harmonic signal, which includes the effect of nuclear vibration, is generally stronger by 1–2 orders of magnitude than that for the nuclei fixed at the equilibrium distance $R = 2$ a.u., particularly in the low-energy and central parts of the spectrum [Fig. 4(a)]. Only in the high-energy part of the spectrum (harmonic orders 40–50) do the two signals get close to each other. On the contrary, a comparison with the HHG spectrum for the nuclei fixed at $R = 2.4$ a.u.

[Fig. 4(b)] shows better agreement for low harmonics (harmonics orders 3–20), while in the high-energy part of the spectrum the fixed-nuclei signal is 1–2 orders of magnitude stronger. The larger the internuclear separation in the ground electronic state of H_2^+ , the smaller the vertical ionization potential is. Decreased ionization potential means enhanced ionization in the laser field. Then the HHG is also enhanced according to the three-step model [30]. Thus there is no surprise that the HHG signal in the fixed-nuclei approximation is stronger at $R = 2.4$ a.u. than at $R = 2$ a.u. When the laser-induced nuclear vibration is taken into account, the molecule spends a substantial amount of time in the stretched configuration, where the internuclear distance is larger than the equilibrium value of $R = 2$ a.u. Therefore, the HHG signal of the vibrating molecule is generally stronger than that for the fixed internuclear distance $R = 2$ a.u. However, the results presented in Fig. 4 suggest also that different instantaneous internuclear distances (hence different time moments during the laser pulse) may be responsible for different parts of the HHG spectrum. Deeper insight into this matter is provided by the time-frequency analysis of the dipole acceleration by means of the wavelet transformation [31]

$$\tilde{a}_w(\omega, t) = \sqrt{\omega} \int_{-\infty}^{\infty} dt' W[\omega(t' - t)] a(t'). \quad (29)$$

For our purposes, the natural choice of the mother wavelet $W(x)$ is the Morlet wavelet

$$W(x) = \exp(ix) \exp\left(-\frac{x^2}{2\tau^2}\right), \quad (30)$$

so Eq. (29) represents a type of short-time Fourier transform. For the window width parameter τ , we use the value $\tau = 15$, previously tested and adopted for the time-frequency analysis of HHG signals [11,32].

In Fig. 5 (top panel) we show the absolute value $|\tilde{a}_w(\omega, t)|$ of the time-frequency distribution calculated for H_2^+ initially in the ground state ($v = 0$). As one can see, the low harmonics (orders 3–7) are generated with substantial intensity over a long time interval (4–8 OCs), with the maximum of the distribution approximately at $t = 7$ OCs, when the internuclear distance reaches its largest value. For the harmonics 9–15, the maximum production times are 7–8 OCs. For the plateau harmonics with the orders 19–45, the maximum of the distribution is gradually shifted from 7 to 6 OCs when the harmonic order is increased. Thus the highest harmonics are mainly generated when the instantaneous laser field intensity is close to its peak value while the vertical ionization potential of H_2^+ is quite large. On the contrary, the lower harmonics are predominantly produced at smaller values of the vertical ionization potential (and larger internuclear separations), although the laser field is not the strongest at those times. Therefore, the time-frequency analysis is in agreement with the observations based on the comparison of the HHG spectra for the vibrating and fixed nuclei (Fig. 4). For comparison, we also show in Fig. 5 (bottom panel) the time-frequency spectrum for H_2^+ with the nuclei fixed at the equilibrium distance $R = 2$ a.u. As one can see, in this case the maximum production of all harmonics is reached close to the peak intensity of the laser field at 5 OCs. An exception is made by a line near the harmonic order 7.5. This line is due to the resonance with the $1\sigma_u$ electronic state at

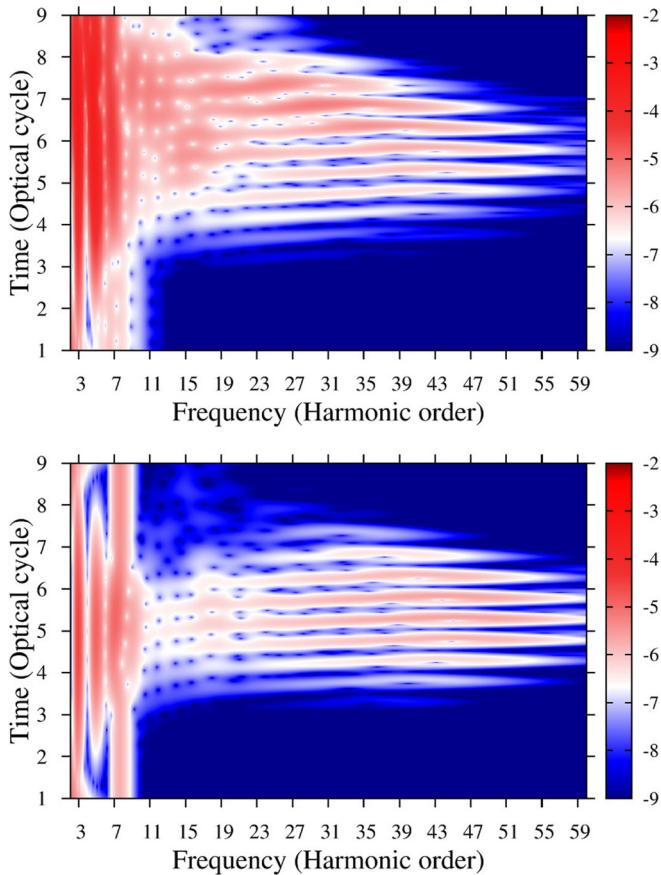


FIG. 5. (Color online) Time-frequency spectrum of dipole acceleration $|\ddot{\alpha}_w(\omega, t)|$ for H_2^+ initially in the ground state ($v=0$) for the peak intensity of the laser field 2×10^{14} W/cm² (top) and the analogous spectrum for H_2^+ with the nuclei fixed at $R=2$ a.u. (bottom). The color scale is logarithmic.

$R=2$ a.u.; it remains strong even at low intensities of the external field. This line is not well pronounced for the vibrating molecule (Fig. 5, top panel) since the resonance conditions are

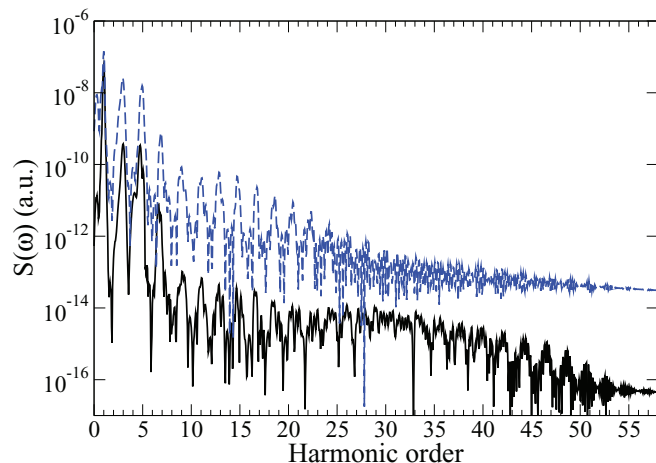


FIG. 6. (Color online) Plot of the HHG spectra of H_2^+ initially in the vibrational states $v=0$ (solid black line) and $v=1$ (dashed blue line), for the peak intensity of the laser field 2×10^{14} W/cm².

not satisfied when the nuclei are shifted from their equilibrium positions.

In Fig. 6 we compare the HHG spectra for the initial vibrational states $v=0$ and 1. The spectral density for $v=1$ is 2–3 orders of magnitude larger than that for $v=0$. We can explain such a significant enhancement of the HHG for $v=1$ by a much larger magnitude of nuclear vibration in this state. As can be seen in Fig. 3, under the influence of the laser pulse, the nuclear density distribution is spread to the internuclear distances of 3–4 a.u., with a substantial portion of dissociative wave packet at even larger distances. The vertical ionization potential of the ground electronic state of H_2^+ changes from 1.103 a.u. at $R=2$ a.u. to 0.796 a.u. at $R=4$ a.u. Since HHG is a highly nonlinear process, such a considerable decrease of the vertical ionization potential results in the dramatic enhancement of the harmonic signal.

IV. CONCLUSION

In this paper we have studied the effect of nuclear vibration on HHG in the H_2^+ molecular ion. We have solved the time-dependent Schrödinger equation for H_2^+ in the laser field with three spatial coordinates, including the nuclear vibration on the same footing as the electronic degrees of freedom. Our results reveal a striking difference of HHG in vibrating molecules and that in molecules with the fixed nuclei. For the ground vibrational level ($v=0$) as the initial state, the lower-energy part of the HHG spectrum is considerably enhanced compared with the spectrum for the nuclei fixed at the equilibrium separation $R=2$ a.u. The enhancement is due to the contribution of larger internuclear separations during the molecular vibration in the laser field where the vertical ionization potential is lower than that at the equilibrium internuclear distance. This finding is confirmed by the time-frequency analysis of the laser-induced dipole acceleration, performed by means of the wavelet transformation. The HHG signal throughout the whole spectrum is much stronger for the H_2^+ molecules initially in the first excited vibrational state ($v=1$) than for the ground initial state ($v=0$). Again, we attribute this effect to the contributions of larger internuclear separations. In the case $v=1$, the vibration during the laser pulse is extended towards larger internuclear distances than in the case $v=0$. Consequently, the molecule spends more time in the stretched configurations with the small vertical ionization potential where both multiphoton ionization and HHG are enhanced.

Our present results are obtained for H_2^+ , the simplest one-electron molecule. In multielectron diatomic molecules, the effect of nuclear vibration on HHG can also be very significant. Our theoretical and computational method can be extended for the study of multielectron diatomic molecules described within the time-dependent density-functional theory [26,33], which is beyond the scope of the present paper.

ACKNOWLEDGMENTS

This work was partially supported by the Chemical Sciences, Geosciences and Biosciences Division of the Office of Basic Energy Sciences, Office of Sciences, US Department of Energy. We also acknowledge partial support from

the Ministry of Science and Technology of Taiwan and National Taiwan University (Grants No. 103R104021 and

No. 103R8700-2). D.A.T. acknowledges partial support from St. Petersburg State University (Grant No. 11.38.654.2013).

-
- [1] F. Krausz and M. Ivanov, *Rev. Mod. Phys.* **81**, 163 (2009).
- [2] M. Hentschel, R. Kienberger, C. Spielmann, G. A. Reider, N. Milosevic, T. Brabec, P. Corkum, U. Heinzmann, M. Drescher, and F. Krausz, *Nature (London)* **414**, 509 (2001).
- [3] P. M. Paul, E. S. Toma, P. Breger, G. Mullot, F. Augé, P. Balcou, H. G. Muller, and P. Agostini, *Science* **292**, 1689 (2001).
- [4] J. Itatani, J. Levesque, D. Zeidler, H. Niikura, H. Pépin, J. C. Kieffer, P. B. Corkum, and D. M. Villeneuve, *Nature (London)* **432**, 867 (2004).
- [5] W. Li, X. Zhou, R. Lock, S. Patchkovskii, A. Stolow, H. C. Kapteyn, and M. M. Murnane, *Science* **322**, 1207 (2008).
- [6] J. H. Posthumus, *Rep. Prog. Phys.* **67**, 623 (2004).
- [7] M. Lein, *J. Phys. B* **40**, R135 (2007).
- [8] M. Lein, N. Hay, R. Velotta, J. P. Marangos, and P. L. Knight, *Phys. Rev. A* **66**, 023805 (2002).
- [9] G. L. Kamta and A. D. Bandrauk, *Phys. Rev. A* **71**, 053407 (2005).
- [10] D. A. Telnov and Shih-I Chu, *Phys. Rev. A* **76**, 043412 (2007).
- [11] X. Chu and Shih-I Chu, *Phys. Rev. A* **63**, 023411 (2001).
- [12] D. A. Telnov and Shih-I Chu, *Phys. Rev. A* **71**, 013408 (2005).
- [13] M. Lein, *Phys. Rev. Lett.* **94**, 053004 (2005).
- [14] C. B. Madsen and L. B. Madsen, *Phys. Rev. A* **74**, 023403 (2006).
- [15] C. C. Chirilă and M. Lein, *Phys. Rev. A* **77**, 043403 (2008).
- [16] A. D. Bandrauk, S. Chelkowski, S. Kawai, and H. Lu, *Phys. Rev. Lett.* **101**, 153901 (2008).
- [17] P. P. Corso, E. Fiordilino, and F. Persico, *J. Phys. B* **40**, 1383 (2007).
- [18] M. Y. Emelin, M. Y. Ryabikin, and A. M. Sergeev, *New J. Phys.* **10**, 025026 (2008).
- [19] A. T. Le, T. Morishita, R. R. Lucchese, and C. D. Lin, *Phys. Rev. Lett.* **109**, 203004 (2012).
- [20] L. S. Cederbaum, *J. Chem. Phys.* **128**, 124101 (2008).
- [21] A. Abedi, N. T. Maitra, and E. K. U. Gross, *Phys. Rev. Lett.* **105**, 123002 (2010).
- [22] Z. Zhou and Shih-I Chu, *Phys. Rev. A* **71**, 011402(R) (2005).
- [23] F. Anis and B. D. Esry, *Phys. Rev. A* **77**, 033416 (2008).
- [24] T. Niederhausen, U. Thumm, and F. Martín, *J. Phys. B* **45**, 105602 (2012).
- [25] X. M. Tong and Shih-I Chu, *Chem. Phys.* **217**, 119 (1997).
- [26] D. A. Telnov and Shih-I Chu, *Phys. Rev. A* **80**, 043412 (2009).
- [27] C. C. Marston and G. G. Balint-Kurti, *J. Chem. Phys.* **91**, 3571 (1989).
- [28] L. Hilico, N. Billy, B. Grémaud, and D. Delande, *Eur. Phys. J. D* **12**, 449 (2000).
- [29] L. D. Landau and E. M. Lifshitz, *The Classical Theory of Fields* (Pergamon, Oxford, 1975).
- [30] P. B. Corkum, *Phys. Rev. Lett.* **71**, 1994 (1993).
- [31] C. K. Chui, *An Introduction to Wavelets* (Academic, New York, 1992).
- [32] X.-M. Tong and Shih-I Chu, *Phys. Rev. A* **61**, 021802 (2000).
- [33] J. Heslar, D. Telnov, and Shih-I Chu, *Phys. Rev. A* **83**, 043414 (2011).